ELSEVIER

Catalysis Today 64 (2001) 217–225

CATALYSIS TODAY

www.elsevier.com/locate/cattod

The effects of kinetics, hydrodynamics and feed conditions on methane coupling using fluidized bed reactor

S.M. Al-Zahrani*

Chemical Engineering Department, King Saud University, PO Box 800, Riyadh 11421, Saudi Arabia

Abstract

A previously developed model describing bubbling fluidized bed reactors is used in this investigation to study the effect of various important hydrodynamic, operating and design parameters on the performance of a large scale fluidized bed reactor used in oxidative coupling of methane. Three kinetic schemes obtained from the literature have been used in this study. The model predicted fairly well the experimental results reported recently under different reaction conditions. The simulation results revealed that increasing the ratio of methane to oxygen in the feed leads to lower methane conversion but higher C_2 selectivity. As the ratio is decreased the system loses its fixed-point stability to a periodic stability. Higher methane conversion and product selectivity are obtained upon decreasing the feed flow rate and particle diameter.

Keywords: Methane; Oxidative coupling; Fluidized bed reactors; Ethane; Ethylene; Two-phase theory

1. Introduction

The oxidative coupling of methane (OCM) to produce ethane and ethylene achieved huge interest in the last 15 years. However, further enhancement of the catalytic performance via developing more active and selective catalysts besides reaction engineering aspects are necessary to make this process commercially attractive. Since the methane coupling reaction involves complex reaction mechanisms, it is clear that C_2 selectivity and yield do not depend only on the catalyst but also on the type of the reactor and reaction operating conditions. Therefore, further enhancement in $C_2{}^+$ selectivity and yield by catalyst improvement or appropriate reactor configuration is necessary to make the process commercially viable. The major engineering challenge is to carry out the reaction in a safe manner and to cope with the large amount of heat released in methane coupling process. Fluidized bed reactor seems to be the most promising reactor type for such a process, particularly for processes requiring high conversion of methane. The feasibility of laboratory scale bubbling fluidized bed reactors for methane coupling has been successfully reported [1–5], however, very few papers appeared in the literature which modeled fluidized bed reactors for methane coupling [5,6].

A relatively rigorous model for OCM in a bubbling fluidized bed reactor was recently introduced by Al-Zahrani and Abasaeed [7]. The model which was based on the two-phase theory of fluidization accounts for the mass and heat transfer between the dense phase and the bubble phase, which plays an important role in the OCM process in a fluidized bed reactor. The model takes into account the change in number of moles accompanying the reaction in the dense phase. A comparison of model predictions with data obtained from the literature was also presented and an excellent

* Tel.: +966-1-4676873; fax: +966-1-4678770.
E-mail address: szahrani@ksu.edu.sa (S.M. Al-Zahrani).

0920-5861/01/$ – see front matter
PII: S0920-5861(00)00525-3

Nomenclature

A_b	cross-sectional area of the bubble phase (cm^2)
A_w	surface area of reactor (cm^2)
C_j	concentration of component j in the dense phase (mol/cm^3)
C_{0j}	initial concentration of component j (mol/cm^3)
c_{pg}	molar heat capacity of gas (J/g K)
c_{pgf}	molar heat capacity of feed gas (J/g K)
D	bed diameter (cm)
D_B	bubble diameter (cm)
D_p	catalyst particle diameter (cm)
H	bed height (cm)
ΔH_{Ri}	heat of reaction i (J/mol)
HBP	Hopf bifurcation point
h_{bd}	interphase heat transfer coefficient between bubble and dense phase based on bubble phase volume ($J/(cm^3\,s\,K)$)
h_w	wall heat transfer coefficient ($J/(cm^2\,s\,K)$)
K_{bdj}	interphase mass transfer coefficient between bubble and dense phase for component j based on bubble phase volume (s^{-1})
M	number of reactions
n_{bj}	molar flow rate of component j in bubble phase (mol/s)
n_{dj}	molar flow rate of component j in dense phase (mol/s)
n_{dj0}	initial molar flow rate of component j in dense phase (mol/s)
n_{fj}	molar flow rate of component j in feed phase (mol/s)
n_{j0}	initial molar flow rate of component j in bubble phase (mol/s)
n_{0j}	initial molar flow rate of component j to the reactor (mol/s)
P_j	partial pressure of component j (kPa)
P_T	total pressure (kPa)
Q_b	flow in bubble phase (cm^3/s)
Q_d	volumetric flow in dense phase (cm^3/s)
Q_f	volumetric flow of the feed (cm^3/s)
R	gas constant ($atm\,cm^3/(mol\,K)$)
$-r_{CH_4}$	rate of consumption of methane ($mol/(g_{cat}\,s)$)
r_i	rate for reaction i ($i = 1, 2, 3$) ($mol/(g_{cat}\,s)$)
SPB	stable periodic branch
SSB	static stable branch
T_b	bubble phase temperature (K)
T_{b0}	bubble phase temperature at $z = 0$ (K)
T_d	dense phase temperature (K)
T_{d0}	dense phase temperature at $z = 0$ (K)
T_f	feed gas temperature (K)
T_{ref}	reference temperature (K)
T_w	wall temperature (K)
U_b	bubble velocity (cm/s)
U_{mf}	minimum fluidization velocity (cm/s)
U_0	gas superficial velocity (cm/s)
UPB	unstable periodic branch
V	volume of reactor (cm^3)
y_{dj}	mole fraction of component j in the dense phase
Z1	methane fraction in feed ($CH_4/(CH_4 + O_2)$)
z	distance measured along reactor length (cm)

Greek symbols

δ	fraction of bed consisting of bubbles
ε_{mf}	void fraction at minimum fluidization
μ	viscosity (g/cm s)
ρ_g	density of gas (g/cm^3)
ρ_p	density of solids (g/cm^3)
ρ_{gf}	density of feed gas (g/cm^3)

agreement between the model predictions and the experimental data was obtained as shown in the previous work [7].

Following these encouraging results, the research program was expanded to include reaction engineering studies which have been focused on improving methane conversion and C_2 selectivity to levels required for practical processes in a large scale reaction system. However, to date, no industrial data is available for large scale reactors, and thus, in the present work, the effect of some key parameters (e.g. methane to oxygen ratio in the feed, catalyst particle diameter, feed flow rate and feed temperature) on reactor performance and bifurcation behavior for a non-adiabatic, non-isothermal operation was investigated.

2. The model

The model used in this work is based on the two-phase theory which considers the fluidized bed reactor to consist of a bubble phase and a dense phase. The model applied is characterized by the following assumptions:

1. The bubble gas is devoid of solids and is in plug flow while the extent of reaction in the bubble-cloud phase is negligible.
2. The dense phase is perfectly mixed and uniform in temperature.
3. The ideal gas law applies to the gas phase in both phases.
4. The mass and heat transfer resistances between the particles and the dense phase gas are negligible.

More details can be found elsewhere [7,8]. The material and energy balances in both phases are given below.

2.1. Reaction kinetics

In this investigation, the three kinetic models developed by Geerts et al. [6], Cheng and Shuai [9] and Santamaria et al. [10] are used. The kinetic scheme proposed by Geerts et al. [6] is a simple triangular network as follows:

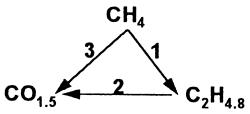

in which the C_2 lump is assumed (following experimental verification) to contain ethane and ethylene in the ratio of 2:3.

The rate equations for this scheme are given as follows:

$$r_1 = 0.016\,\mathrm{e}^{-100/RT} P_{\mathrm{CH_4}}^{0.9} P_{\mathrm{O_2}}^{0.3} \tag{1}$$

$$r_2 = 0.02\,\mathrm{e}^{-70/RT} P_{\mathrm{CH_4}}^{0.5} P_{\mathrm{O_2}}^{1.5} \tag{2}$$

$$r_3 = 0.2\,\mathrm{e}^{-150/RT} P_{\mathrm{C_2}}^{1.4} P_{\mathrm{O_2}}^{0.7} \tag{3}$$

The four-lump kinetic scheme proposed by Cheng and Shuai [9] which differentiates between ethane and ethylene is given as follows:

$$\mathrm{CH_4 + 2O_2 \rightarrow CO_2 + 2H_2O},$$

$$r_1 = 0.015\,\mathrm{e}^{-6134/T} C_{\mathrm{CH_4}}^{0.4} C_{\mathrm{O_2}}^{1.5} \tag{4}$$

$$\mathrm{2CH_4 + 0.5O_2 \rightarrow C_2H_6 + H_2O},$$

$$r_2 = 0.6\,\mathrm{e}^{-11908/T} C_{\mathrm{CH_4}}^{0.8} C_{\mathrm{O_2}}^{1.1} \tag{5}$$

$$\mathrm{C_2H_4 + 2O_2 \rightarrow CO_2 + 2H_2O},$$

$$r_3 = 1.0 \times 10^{-4}\,\mathrm{e}^{-722/T} C_{\mathrm{C_2H_6}}^{0.8} C_{\mathrm{O_2}} \tag{6}$$

$$\mathrm{C_2H_6 + 0.5O_2 \rightarrow C_2H_4 + H_2O},$$

$$r_4 = 1.0 \times 10^{-16}\,\mathrm{e}^{-26461/T} C_{\mathrm{C_2H_4}}^{0.8} C_{\mathrm{O_2}}^{1.6} \tag{7}$$

The kinetic scheme proposed by Santamaria et al. [10] considers both the gas phase as well as the catalytic reactions and is given by Eqs. (8)–(10) and Eqs. (11)–(13), respectively. This can be achieved by using the following lumped kinetic model:

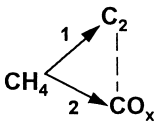

where C_2 represents the total amounts of hydrocarbons with two or more carbon atoms and CO_x represents the total amounts of carbon oxides.

Gas-phase kinetics:

$$-r_{\mathrm{CH_4}} = -\frac{\mathrm{d}C_{\mathrm{CH_4}}}{\mathrm{d}t} = 7.607 \times 10^5\,\mathrm{e}^{-27600/T} C_{\mathrm{CH_4}}^{1.04} C_{\mathrm{O_2}}^{2.05} T^{3.09} \tag{8}$$

$$r_1 = \frac{\mathrm{d}C_{\mathrm{CO}_x}}{\mathrm{d}t} = 1.29 \times 10^9\,\mathrm{e}^{-36100/T} C_{\mathrm{CH_4}}^{0.53} C_{\mathrm{O_2}}^{3.7} T^{4.23} + 0.622\,\mathrm{e}^{-14900/T} C_{\mathrm{CH_4}}^{-0.95} C_{\mathrm{O_2}}^{1.33} T^{0.38} \tag{9}$$

$$r_2 = \frac{\mathrm{d}C_{\mathrm{C_2}}}{\mathrm{d}t} = 5.367 \times 10^4\,\mathrm{e}^{-26100/T} C_{\mathrm{CH_4}}^{1.04} C_{\mathrm{O_2}}^{1.78} T^{2.82} + 1.464 \times 10^4\,\mathrm{e}^{-26200/T} C_{\mathrm{CH_4}}^{1.16} C_{\mathrm{O_2}}^{1.62} T^{2.78} \tag{10}$$

Catalytic kinetics:

$$-r_{CH_4} = -\frac{dC_{CH_4}}{dt} = 2.176 \times 10^{18}\, e^{-42700/T} C_{CH_4}^{1.05} C_{O_2}^{0.4} + 8.04 \times 10^{9}\, e^{-20050/T} C_{CH_4}^{0.55} C_{O_2}^{1.04} \quad (11)$$

$$r_1 = \frac{dC_{CO_x}}{dt} = 8.04 \times 10^{9}\, e^{-20050/T} C_{CH_4}^{0.55} C_{O_2}^{1.04} \quad (12)$$

$$r_2 = \frac{dC_{C_2}}{dt} = 1.088 \times 10^{18}\, e^{-42700/T} C_{CH_4}^{1.05} C_{O_2}^{0.4} \quad (13)$$

2.2. Material and energy balances in the bubble phase

The material and energy balance equation for the j component in the bubble phase of the fluidized bed reactor at steady state are given below.

Material balances:

$$\frac{dn_{bj}}{dz} = K_{bdj} A_b \left(\frac{n_{dj}}{Q_d} - \frac{n_{bj}}{Q_b} \right) \quad (14)$$

at $z = 0$, $n_{bj} = n_{bj0}$ and $n_{dj} = n_{dj0}$.

Energy balance:

$$\rho_g c_{pg} U_b \frac{dT_b}{dz} = h_{bd}(T_d - T_b) \quad (15)$$

at $z = 0$, $T_b = T_{b0}$ and $T_d = T_{d0}$ (note: $T_{b0} = T_{d0} = T_f$, feed temperature).

2.3. Material and energy balances in the dense phase

The steady state dense phase material and energy balances are given below.

Material balances:

$$n_{dj} = n_{dj0} + \int_0^H K_{bdj} \left(\frac{n_{bj}}{Q_b} - \frac{n_{dj}}{Q_d} \right) A_b\, dz + V(1-\delta)(1-\varepsilon_{mf})\rho_p \sum_{i=1}^{M} \alpha_{ij} r_i \quad (16)$$

where α_{ij} are the stoichiometric coefficients (negative for reactants, positive for products and zero for components not appearing in reaction), r_i are the reaction rates and M is the number of reactions. The integral in Eq. (16) is evaluated from the bubble phase, Eq. (14), thus giving Eq. (17).

$$n_{dj} = n_{dj0} + U_b A_b \left(\frac{n_{0j}}{Q_f} - \frac{n_{dj}}{Q_d} \right) (1 - e^{-\gamma_j H}) + V(1-\delta)(1-\varepsilon_{mf})\rho_p \sum_{i=1}^{M} \alpha_{ij} r_i \quad (17)$$

where $\gamma_j = K_{bdj}/U_b$, $n_{bjf}/Q_b = n_{0j}/Q_f =$ feed concentration.

From the ideal gas law $y_{dj} P Q_d = n_{dj} R T_d$. Therefore, the change in volumetric flow rate in the dense phase resulting from the change in the number of moles due to the reaction is given by

$$Q_d = \frac{\sum n_{dj} R T_d}{P} \quad (18)$$

Energy balance:

$$\rho_{gf} Q_{d0} c_{pgf}(T_f - T_{ref}) - \rho_g Q_d c_{pg}(T_d - T_{ref}) - \int_0^H h_{bd}(T_b - T_d) A_b\, dz + V(1-\delta)(1-\varepsilon_{mf})\rho_p \times \sum_{i=1}^{M} (-\Delta H_{Ri}) r_i - h_w A_w (T_d - T_w) = 0 \quad (19)$$

The integral in Eq. (19) is evaluated from Eq. (15) to give Eq. (20):

$$\rho_{gf} Q_{d0} c_{pgf}(T_f - T_{ref}) - \rho_g Q_d c_{pg}(T_d - T_{ref}) - U_b A_b \rho_g c_{pg}(T_f - T_d)(1 - e^{-\beta H}) + V(1-\delta)(1-\varepsilon_{mf})\rho_p \sum_{i=1}^{M} (-\Delta H_{Ri}) r_i - h_w A_w (T_d - T_w) = 0 \quad (20)$$

where

$$\beta = \frac{h_{bd}}{U_b \rho_g c_{pg}}$$

3. Results and discussion

Sensitivity analysis was carried out to assess the effect of the various design, operating as well as hydrodynamic parameters on the reactor performance and the bifurcation behavior of the system. The efficient AUTO86 software [11] was used to construct the bifurcation diagrams. To ensure accuracy of the results,

Table 1
Values of parameters used in simulation

Parameter	Value
H (cm)	230
D_p (cm)	0.0075
T_f (K)	973
P_T (atm)	1
D (cm)	460
ρ_p (g/cm^3)	1.3
T_w (K)	303
U_0/U_{mf}	7.5

Table 2
Comparison of model predictions using the three kinetic schemes

	Geerts et al. [6]	Cheng and Shuai [9]	Santamaria et al. [10]
T_d (K)	1051	1089	1337
CH_4 conversion (%)	31.90	31.76	25.02
C_2 selectivity (%)	84.5	87.1	83.1
C_2 yield (%)	27.0	27.8	20.7
C_2H_6/C_2H_4	0.67	0.57	0.670

the bound on allowable error was maintained at 10^{-12} throughout the calculations. The reactor design parameters as well as operating conditions for the base case used in the simulations are listed in Table 1. The heat capacities, diffusivity, the density of the gas, and heats of reactions are function of dense phase temperature.

The comparison between the three kinetic schemes reported by Geerts et al. [6], Cheng and Shuai [9] and Santamaria et al. [10] employed in this study is summarized in Table 2 using the parameter values given for the base case and listed in Table 1. In this comparison the differences in catalysts properties are taken into consideration. As shown in Table 2 the simple triangular kinetics of Geerts et al. [6] gave comparable results to the four-lump kinetics reported by Cheng and Shuai [9]. The dense phase temperature predicted by the kinetics of Santamaria et al. [10], which considers both the gas-phase as well as the catalytic reaction, is higher than that predicted by the other two schemes. The ratio of C_2H_4 to C_2H_6 for all kinetic schemes is very close to that assumed by Geerts et al. [6] which underscores the applicability of the other kinetics. Therefore, the kinetics of Geerts et al. [6] is tested against the experimental data of Pannek and Mleczko [5] and parametric study using this kinetics is also conducted as will be shown in the following

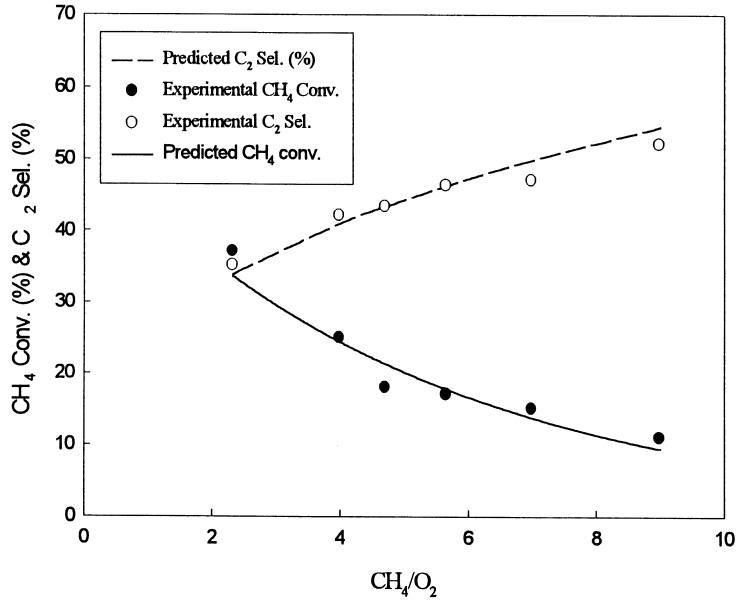

Fig. 1. Comparison between the model predictions (lines) and experimental results of Pannek and Mleczko [5] (symbols) for methane conversion and C_2 selectivity vs CH_4:O_2 in the feed at $T = 1023$ K.

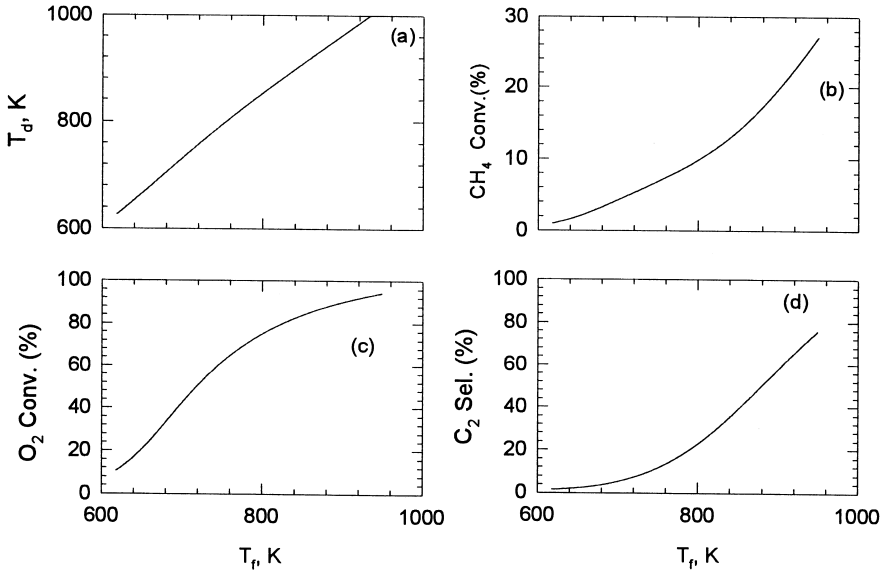

Fig. 2. The effect of feed temperature on: (a) dense phase temperature; (b) methane conversion; (c) oxygen conversion; (d) C_2 selectivity.

sections. For the sake of comparison, the reactor dimensions and operating conditions are adjusted according to experimental conditions ($H = 6$ cm, $D = 7$ cm ID, $U_0/U_{mf} = 20$, $D_p = 120\,\mu$m, $P_T = 100$ kPa). As shown in Fig. 1, very good agreement between model predictions and experimental values has been obtained for both methane conversion and C_2 selectivity. Fig. 1 also illustrates the trends observed during OCM reactions, i.e. as conversion increases, the selectivity decreases.

3.1. Effect of feed temperature

Fig. 2 shows the predicted steady state values of the dense phase temperature, CH_4 conversion, O_2 conversion, and C_2 selectivity at different feed temperatures. The steady state dense phase temperature increases almost linearly with increasing the feed temperature as illustrated in Fig. 2a. Methane conversion also increases with increasing the feed temperature and it reaches about 28% conversion at a feed temperature of 940 K as shown in Fig. 2b. At higher feed temperature the oxygen is almost converted as shown in Fig. 2c. Fig. 2d shows the increase of the C_2 selectivity with increasing feed temperature. These results are in good agreement with the experimental investigations for different catalysts reported recently [1–3]. The increase in C_2 selectivity with growing dense phase temperature results from the higher activation energy of the selective, primary reaction step.

3.2. Effect of feed molar distribution

Fig. 3 shows the bifurcation diagram for the reactor dense temperature (T_d) with the fraction of methane in the feed (Z1) as the bifurcation parameter. It is clear from Fig. 3a that as the methane fraction in the feed is decreased, the reactor dense phase temperature increases in a stable manner (the solid line) due to the increase of the amount of available oxygen which enhances the exothermic reactions (the CO_x formation). At Z1 about 0.7723, a Hopf bifurcation point (HBP, ■) appears which indicates transition from stable fixed point steady states to unstable fixed points steady states (the dashed line). This unstable point attractors are surrounded by stable periodic attractors (limit cycles, shown by the symbols, ●) as shown in the enlargement given in Fig. 3b. The oscillatory behavior in the range $0.7665 < Z1 < 0.7723$ resembles the oscillations which are obtained experimentally for CO reactions [12]. The oscillations of the dense phase temperature increases as the bifurcation parameter is

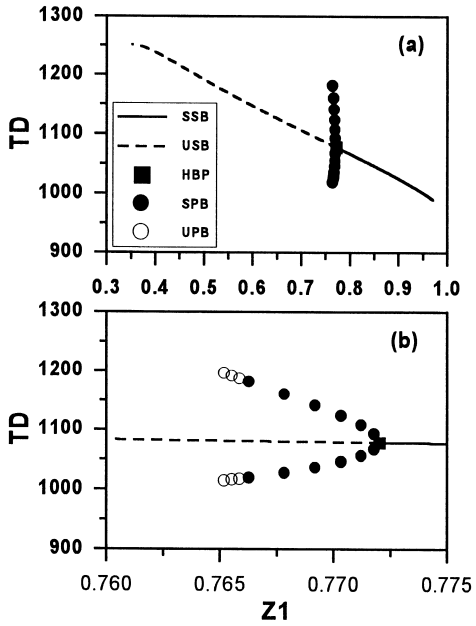

Fig. 3. The effect of methane fraction (Z1) in the feed on: (a) dense phase temperature; (b) enlargement of the periodic branch.

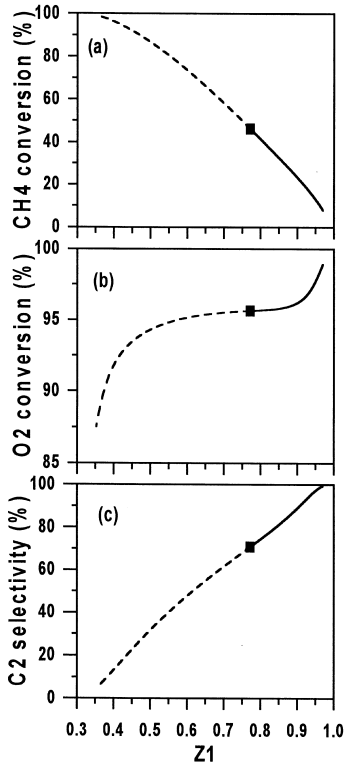

Fig. 4. The effect of methane fraction (Z1) in the feed on: (a) methane conversion; (b) oxygen conversion; (c) C_2 selectivity.

decreased to about 1000 < TD < 1180. These stable limit cycles become unstable (shown by the symbol ○) as the bifurcation parameter is decreased below 0.7665.

As the amount of methane in the feed (Z1) is decreased, the methane conversion increases from about 10% to about 46.2% at the Hopf bifurcation point, however the conversion of oxygen decreases to about 95.6% and the C_2 selectivity drops to about 70% as seen from Fig. 4a–c, respectively.

3.3. Effect of feed volumetric flow rate

To date, the experimental investigation on OCM has been conducted in small-fluidized bed reactors that have been operated in the bubbling bed regime with U_0/U_{mf} in the range 5–11 [2,3,13]. As shown in Fig. 5, lower U_0/U_{mf} ratios tend to favor methane conversion, oxygen conversion and C_2 selectivity at the expense of higher dense phase reaction temperature. A plausible explanation for these enhancements is that as U_0/U_{mf} is decreased the residence time in the reactor increases.

3.4. Effect of particle diameter

Another important parameter which affects both the reaction and the hydrodynamics of fluidized bed reactors is the particle diameter (D_p). Therefore its effect on the performance of the system was investigated for particle sizes range 100–800 μm. Fig. 6a reveals that decreasing the particle size enhances the reaction thus giving increased values of reaction temperature. Methane conversion, oxygen conversion and C_2 selectivity are also enhanced by decreasing the catalyst particle size as illustrated in Fig. 6b–d, respectively. Particle diameter variations affect the minimum fluidization velocity U_{mf} and consequently the mass transfer exchange parameter, K_{bd}. These results are in agreement with the experimental results in a small laboratory scale fluidized bed reactor reported by Mleczko et al. [14], who observed that for the whole range of investigation for catalyst particle size the

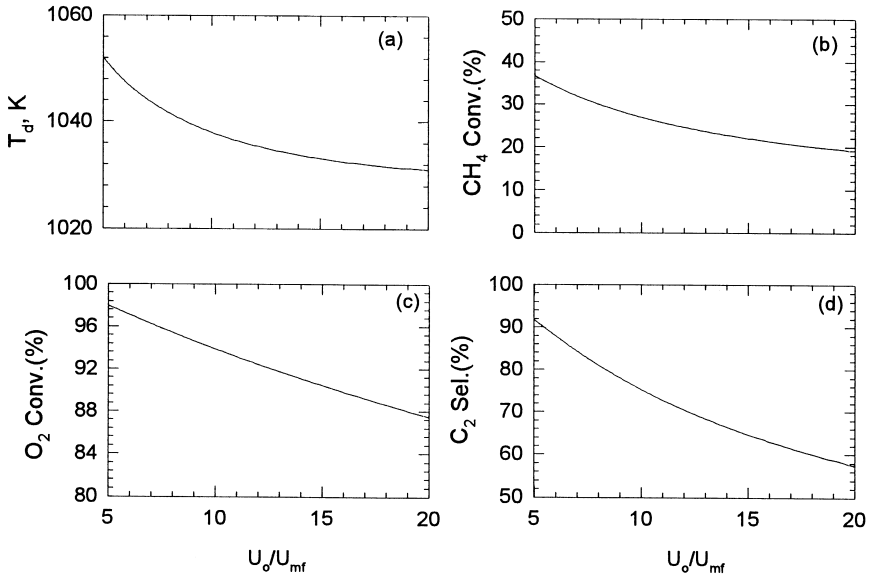

Fig. 5. The effect of superficial velocity on: (a) dense phase temperature; (b) methane conversion; (c) oxygen conversion; (d) C_2 selectivity.

reaction temperature, methane conversion and C_2 selectivity increase with decreasing the particle diameter. However, it is important to mention that while small particle size enhances the reactor performance, very small particle sizes are very difficult to use in practice because the intra-particle forces will have larger influence than the gravitational force and therefore gas channeling may occur in the bed and problems associated with particle fluidization may be experienced.

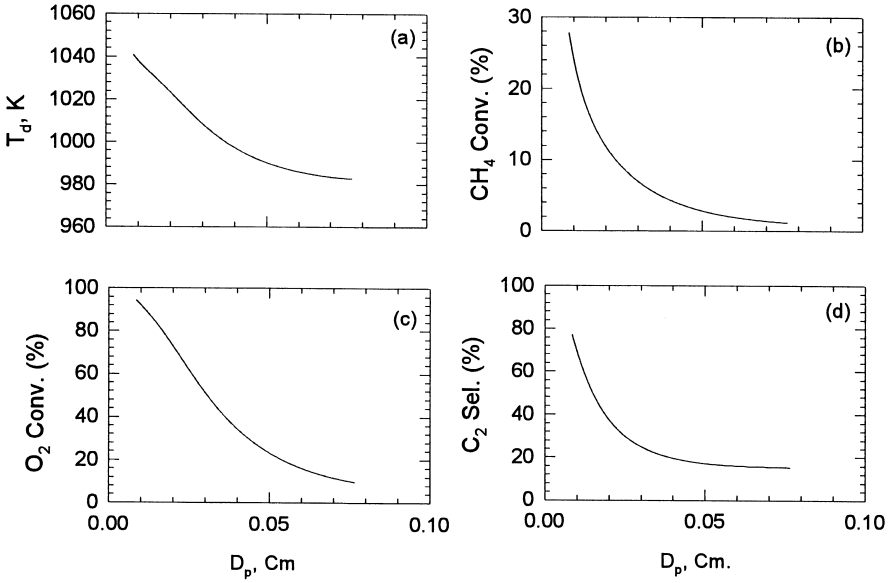

Fig. 6. The effect of particle diameter on: (a) dense phase temperature; (b) methane conversion; (c) oxygen conversion; (d) C_2 selectivity.

4. Conclusions

In this paper various kinetic schemes have been employed to investigate the effect of various important hydrodynamic, operating and design parameters on the performance of fluidized bed reactor used in OCM. A previously developed model describing bubbling fluidized bed reactors is used in this investigation. The model predictions compared favorably with the recent experimental data obtained from the literature. The results reveal that the ratio of methane to oxygen in the feed has a very profound effect on the system performance. Oscillatory operation has been found to occur as the amount of methane in the feed is decreased. Even though increasing the feed temperature leads to higher methane conversion and higher selectivity in the range of investigation, it is advisable to operate at lower feed temperature in order to fully utilize the advantages inherent with fluidized bed systems and to prevent any further oxidation of the C_2 products. While decreasing the feed flow rate (U_0/U_{mf}) and catalyst particle diameter enhances the conversion and selectivity care must be taken to avoid particle agglomeration and gas channeling problems.

References

[1] R. Andorf, M. Baerns, Catal. Today 6 (1990) 445.
[2] J.H. Edwards, K.T. Do, J.H. Tyler, Catal. Today 6 (1990) 435.
[3] J.H. Edwards, J.R. Tyler, S.D. White, Catal. Today 4 (1990) 85.
[4] A. Santos, J. Santamaria, M. Menendez, Ind. Eng. Chem. Res. 34 (1995) 1581.
[5] U. Pannek, L. Mleczko, Chem. Eng. Sci. 51 (1996) 3575.
[6] J.W. Geerts, J.H. Hoebink, K. Van der Wiele, in: L.F. Albright, B.L. Crynes, S. Nowak (Eds.), Novel Production Methods for Ethylene, Marcel Dekker, New York, 1991, p. 207 (Chapter 11).
[7] S.M. Al-Zahrani, A.E. Abasaeed, Dev. Chem. Eng. Mineral Process. 6 (1998) 197.
[8] S.M. Al-Zahrani, A.E. Abasaeed, in: Proceedings of the 16th IASTED International Conference, Gold-Coast, Australia, May 6–9, 1996, pp. 406–413.
[9] S. Cheng, X. Shuai, AIChE J. 41 (1995) 1589.
[10] J.M. Santamaria, E.E. Miro, E.E. Wolf, Ind. Eng. Chem. Res. 30 (1991) 1157.
[11] E.J. Doedel, J.P. Kernevez, Auto Software, California Institute of Technology, Pasadena, CA, 1986.
[12] L.F. Razon, R.A. Schmitz, Catal. Rev. Sci. Eng. 28 (1986) 89.
[13] D. Kunii, O. Levenspiel, Fluidization Engineering, Wiley, New York, 1977, pp. 130–133, 181–219.
[14] L. Mleczko, R. Andorf, M. Baerns, J. Chem. Eng. Technol. 14 (1991) 325.